ARTICLE

H. P. Grimm · A. B. Verkhovsky · A. Mogilner
J.-J. Meister

Analysis of actin dynamics at the leading edge of crawling cells: implications for the shape of keratocyte lamellipodia

Abstract Leading edge protrusion is one of the critical events in the cell motility cycle and it is believed to be driven by the assembly of the actin network. The concept of dendritic nucleation of actin filaments provides a basis for understanding the organization and dynamics of the actin network at the molecular level. At a larger scale, the dynamic geometry of the cell edge has been described in terms of the graded radial extension model, but this level of description has not yet been linked to the molecular dynamics. Here, we measure the graded distribution of actin filament density along the leading edge of fish epidermal keratocytes. We develop a mathematical model relating dendritic nucleation to the long-range actin distribution and the shape of the leading edge. In this model, a steady-state graded actin distribution evolves as a result of branching, growth and capping of actin filaments in a finite area of the leading edge. We model the shape of the leading edge as a product of the extension of the actin network, which depends on actin filament density. The feedback between the actin density and edge shape in the model results in a cell shape and an actin distribution similar to those experimentally observed. Thus, we explain the stability of the keratocyte shape in terms of the self-organization of the branching actin network.

Keywords Actin dynamics · Cell motility · Dendritic nucleation model · Keratocyte · Lamellipodium

A. Mogilner (✉)
Department of Mathematics and Center for Genetics and Development, University of California,
Davis, CA 95616, USA
E-mail: mogilner@math.ucdavis.edu
Fax: +1-530-7526635

H. P. Grimm · A. B. Verkhovsky · J.-J. Meister
Cellular Biophysics and Biomechanics Laboratory,
Swiss Federal Institute of Technology,
1015 Lausanne, Switzerland

Introduction

The crawling motion of animal cells over a substrate has been described as the succession of protrusion, attachment and retraction (Abercrombie 1980). The first step in this sequence, protrusion, is believed to be driven by polymerization of actin at the leading edge of the cell (Condeelis 1993; Mogilner and Oster 1996; Miyata et al. 1999). One of the common types of protrusive specialization of the edge of the cell is the lamellipodium: a flat, leaf-like extension filled with a dense actin network. Recently, significant progress has been made in understanding the molecular events of protrusion and the ultrastructural organization of the growing actin network in the lamellipodia (Borisy and Svitkina 2000; Pollard et al. 2000).

A crucial factor for protrusion is actin polarity. The two ends of an actin filament are structurally and functionally different, one termed barbed (with fast dynamics, favored for polymerization) and the opposite, termed pointed. The principal reactions constituting the cycle of turnover of the lamellipodial actin network are dendritic nucleation, elongation, capping and disassembly of actin filaments. First, proteins of the WASP/Scar families activate Arp2/3 protein complexes. These complexes nucleate new actin filaments at the sides or tips of existing filaments. Nucleation is sterically precise, so the nascent filaments in the network arise in the form of branches off preexisting filaments with the barbed end being free (Welch et al. 1997; Svitkina and Borisy 1999; Borisy and Svitkina 2000; Pollard et al. 2000). The newly formed filaments elongate at their barbed ends, pushing the membrane at the leading edge forward until they are capped. This involves capping proteins that bind to barbed filament ends and block further addition of actin monomers, thus eliminating these ends from the process of protrusion. Actin subunits for the elongation of the uncapped barbed ends are produced in the process of disassembly at the opposite, pointed ends. The disassembly is slow in vitro, but is accelerated in cells by

proteins of the ADF/cofilin family. These proteins increase the number of depolymerizing minus ends in the actin network, resulting in a more efficient replenishing of the subunit pool for filament elongation. Note that the reactions of barbed ends elongation and minus ends depolymerization for a filament are separated in time and space. Capping is believed to further increase the subunit pool by a funnelling effect, restricting the number of growing filament ends, and thus makes the elongation of the remaining uncapped filaments more efficient (Carlier and Pantaloni 1997; Pantaloni et al. 2001; Mogilner and Edelstein-Keshet 2002). During steady locomotion, elongation/disassembly and branching/capping reactions are expected to be balanced, so that the total concentration of polymerized actin as well as the average number of actin filaments does not change.

The turnover of the branching actin network is eventually translated into advancement of the leading edge. Experimentally, it was shown that the polymerization of actin filaments is able to deform vesicles (Cortese et al. 1989) or liposomes (Miyata et al. 1999) and to drive the motion of bacteria and plastic beads in a solution containing purified components of actin-polymerizing machinery (Loisel et al. 1999; Cameron et al. 2001). The elastic polymerization ratchet model (Mogilner and Oster 1996) describes the protrusion mechanism based on the idea that a filament is involved in Brownian motion and consequently undulates and bends very frequently. When a filament is bent, a gap appears between its tip and the cell membrane. If a large enough gap persists for a sufficiently long time interval, a monomer can intercalate into the gap and assemble onto the tip of the growing polymer. This increases fiber length so that when the longer polymer's tip contacts the membrane again, the fiber remains bent and the corresponding elastic force pushes the membrane forward. The model provides the corresponding force–velocity relation and predicts that the filament growth and membrane advance are optimal when the filaments are oriented at an oblique angle to the membrane interface (Mogilner and Oster 1996). The model is supported by a few experiments establishing correlations between the rate of protrusion and the morphology of actin network as well as concentrations of specific molecules involved in actin polymerization (Rinnerthaler et al. 1991; Abraham et al. 1999; Dai and Sheetz 1999; Loisel et al. 1999; Rottner et al. 1999; McGrath et al. 2000; Cameron et al. 2001). Recently, the theory of protrusion mechanics was developed further: both configurations of actin network growing against an obstacle and force–velocity relationships for different branching and capping models were analyzed (Carlsson 2001), and effects of the actin network elasticity were investigated (Gerbal et al. 2000).

Maly and Borisy (2001) analyzed the competition between elongation and capping using a population dynamics theory applied to families of branching filaments oriented at different angles to the leading edge. They showed theoretically and confirmed experimentally that filament families with mother and daughter filaments oriented symmetrically with respect to the direction of the protrusion have the best chances to "survive". Given the branching angle of ~70° (Borisy and Svitkina 2000; Pollard et al. 2000), the predominant filament family is the one with filaments oriented at $\pm 35°$ to the direction of protrusion. Thus, the dynamics and organization of the advancing lamellipodia can be schematically described as rapid turnover of the dendritic actin network, in which the filaments are preferentially oriented at $\pm 35°$ to the direction of protrusion.

The microscopic description of actin organization and dynamics is not sufficient to understand the organization and dynamics of the leading edge at a larger scale, e.g. it does not explain how the overall shape of the leading edge evolves and is controlled by the cell. Relation of the actin dynamics to the geometry of a rigid surface on which the actin network is growing was investigated by Bernheim-Groswasser et al. (2002). However, no analysis is available for the advancing lamellipodium of the moving cell. To answer the question about the relationship between actin dynamics and cell shape, it is useful to consider a model system with well-defined leading edge dynamics. The cells of choice are fish epidermal keratocytes which crawl on surfaces with remarkable speed and persistence while almost perfectly maintaining their characteristic fan-like shape (Lee et al. 1993a) (see also Figs. 2, 3). The front, advancing part of the keratocyte is represented by the lamellipodium, which is only a few tenths of a micrometer thick but stretches for several tens of micrometers from side to side and for about ten micrometers from front to back.

The actin network in the major part of the keratocyte lamellipodium is stationary with respect to the substratum while the cell moves forward. This implies that the rate of the protrusion equals the rate of actin polymerization at the front edge (Theriot and Mitchison 1991; Mitchison and Cramer 1996). In the moving coordinate system of the cell, actin filaments move back from the leading edge, and the barbed ends of the filaments oriented obliquely to the leading edge experience lateral drift along the edge (Small 1994). The density of the actin network decreases from the front to the back of the lamellipodium due to gradual depolymerization of actin as it moves away from the edge (Svitkina et al. 1997; Edelstein and Ermentrout 2000). Only at the lateral and rear extremities of the lamellipodium do actin filaments move with respect to the substratum and to each other. This occurs when they participate in myosin-driven contraction, which has been implicated in forward translocation of the rear part of the keratocyte and in limiting the lateral spreading of the cell (Lee et al. 1993b; Svitkina et al. 1997; Anderson and Cross 2000). Thus, the processes of actin polymerization and the subsequent contraction of the network are spatially separated, and the shape of the front part of the lamellipodium may be considered to be the result of the polymerization-driven protrusion.

Geometrically, the advancing lamellipodium can be described by attributing the normal velocity of protrusion to every point of the leading edge (Lee et al. 1993b). For the shape of a convex lamellipodium to be conserved in the process of locomotion, this normal velocity has to be precisely controlled in space: maximum velocity is expected at the center of the leading edge, with gradual decrease towards the lateral edges. This behavior has been described as graded radial extension (Lee et al. 1993b), but the control of the protrusion rate has yet to be related to the molecular dynamics of actin polymerization.

In the present paper, we mathematically model the population of polymerizing actin filaments at the leading edge of a lamellipodium, taking into account branching and capping as well as the lateral drift of the barbed ends. We also measure the actin density, validate the model by comparing theoretical predictions with the experimental data, and estimate the capping rate using this comparison. Then, we investigate the relation between actin density and rate of protrusion at the leading edge. Finally, we derive and simulate a self-consistent model of coupled density and shape regulation of the lamellipod, which explains the nature of stability and persistence of cell migration.

Methods

Cell culture and microscopy

Epidermal keratocytes of the black tetra (*Gymnocorymbus ternetzi*) were cultured and stained for F-actin with rhodamine phalloidin after glutaraldehyde fixation as described previously (Svitkina et al. 1997). Phase contrast images of locomoting living cells and fluorescence images of fixed cells were taken using a Nikon Eclipse T300 inverted microscope and a Micromax PB1300 cooled CCD camera (Roper Scientific, Trenton, NJ, USA) operated by Metamorph imaging software (Universal imaging, West Chester, Pa., USA). Sixteen-bit phase contrast and fluorescence images were background-subtracted and fluorescence images were also corrected for the non-uniformity of the illumination field before converting to 8-bit format for further analysis.

Measuring actin densities and shapes of the leading edge

Eight-bit gray scale images of the cells were rotated in order to align the direction of locomotion to the y-axis (used for the mathematical model) and then imported into Matlab. The images were used to detect and digitize the leading edge and to measure fluorescence intensity of stained actin along the leading edge. The detection of the edge in phase contrast images was performed using an active contour ("snakes") algorithm implemented in Matlab.

In fluorescence images, the leading edge was detected using a threshold of 10% of maximal intensity. Subsequently, noise was removed using three dilatation steps followed by the same number of erosion steps. A smooth representation of the leading edge was obtained by fitting a 10th-order polynomial to the pixel coordinates; this was done on a domain of 95% of the total width of the cell, i.e. lateral edges were not included.

The intensity of the fluorescence image (which is proportional to the F-actin density) was evaluated by averaging over patches of 5×5 pixels (pixel size 0.08 μm). One hundred such patches were evaluated along the leading edge at a distance of 0.8 μm from the edge, the x-coordinates of the centers of the patches being equally spaced.

Mathematical modeling and comparison to experimental data

F-actin density profiles

In the limiting cases of slow and fast capping, the ordinary differential equations of the "Mathematical model of actin dynamics" section (below), which describe the stationary F-actin density at the flat leading edge, were solved analytically with the help of standard methods of applied mathematics (Logan 1997). We numerically solved the hyperbolic partial differential equations of the "Mathematical model of actin dynamics" section (below), which describe the F-actin density for a stationary shape of the leading edge. The function $f(x)$ describing the leading edge shape was obtained by scaling the measurements described above. The equations were non-dimensionalized as described in the Appendix. The non-dimensional domain $-1 < x < 1$ was discretized by 40 equidistant grid points. We solved the equations using an explicit forward-time numerical scheme. In order to have numerical stability, the equations describing the left-pointing filaments were solved with a forward-difference scheme, the equations for the right-pointing filaments with a backward-difference scheme (Garcia 1994). The time step was small enough to satisfy the Courant–Friedrichs–Lewy condition for stability of the numerical scheme. Initial actin density was zero. We simulated the model long enough for the asymptotically stable stationary density profile to develop. We compared the results of the measurements and model by fitting the theoretical density profile over the experimental one and using the "eyeball" norm (i.e. no formal optimization algorithm was used). More formal methods, i.e. the numerical least squares fit, proved inconclusive.

Shape of the leading edge

We computed local protrusion rates from the measured shapes using the graded radial extension model and plotted the experimental density–velocity results. The density–velocity relation of the elastic polymerization ratchet model was fitted over the experimental data using the discrete least-squares approximation (Garcia 1994).

Evolution and stability of actin density and leading edge shape

We simulated the coupled dynamics of the actin density and leading edge shape using the following explicit iterative procedure. At each computational step: (1) the actin density was updated using the shape of the front and the finite difference approximation to the partial differential equations of the "Mathematical model of actin dynamics" section (below); (2) the local protrusion velocity was computed using the updated actin density and the formula from the elastic polymerization model; (3) the shape of the leading edge was updated using the graded radial extension formula. We ran these simulations on the grid described above using model parameters that generated good fits to the experimental data. We used a random number generator to simulate the stochasticity of the branching and capping processes.

Mathematical model of actin dynamics

We use mathematical modeling to relate the observed features of the actin density to both the polymerization dynamics of actin filaments and the shape of the lamellipodia. The model is based on the following simplifying assumptions:

1. The lamellipodium is effectively a two-dimensional domain. The shape of its leading edge is convex. The slope of the leading edge is not steep (in the sense explained below).
2. Contraction at the rear and sides of the cell is separated from the protrusion at the front. Specifically, the movement of actin filaments with respect to the substrate near the leading edge is negligible and the actin network at the front can be considered fixed with respect to the surface.

3. Individual actin filaments are straight and oriented at $\pm 35°$ to the direction of the cell movement. Note that the filament's thermal bending required for the elastic polymerization ratchet model is small and can be neglected. We assume that the filament orientation is the same across the central part of the lamellipodium: orientation does not depend on the local normal direction to the cell boundary. The results change little if this assumption is changed in the case of relatively flat cell edge.

4. In the absence of specific indications to the contrary, we assume that the concentration of actin monomers available for polymerization, branching/nucleation complexes (Arp2/3), capping proteins and their activity are distributed uniformly along the leading edge. To account for the finite size of the lamellipodium, we assume that no filaments are nucleated outside of the leading edge interval.

We consider the lamellipodium in a coordinate system moving with the cell. The y-axis is oriented forward, parallel to the direction of motion, and the x-axis is parallel to the leading edge at the center of the lamellipodium (Fig. 1). The point $x = 0$ corresponds to the center of the cell, and $x = \pm L$ are the coordinates of the inner boundaries of the lateral edges of the lamellipodium. The leading edge profile is described by the function $y = f(x,t)$ in this coordinate system.

Straight actin filaments can be labelled by their angle with respect to the forward direction (measured clockwise), θ. The angular distribution of actin filaments at the front of the keratocyte measured and modeled in Maly and Borisy (2001) consists of F-actin at all angles, from $-90°$ to $+90°$. However, this angular distribution reveals two prominent peaks, at approximately $\theta_\pm = \pm 35°$. As a simplification for modelling purposes, we assume a perfect angular order in the actin network, with each filament oriented at $\theta_\pm = \pm 35°$ relative to the direction of motion of the cell.

Mathematically, we describe the actin network with the densities $p^+(x,t)$ and $p^-(x,t)$, (μm^{-1}), of right- ($+35°$) and left- ($-35°$) pointing actin filaments with uncapped barbed ends at the leading edge. Note that $p^\pm(x,t)$ is not the number of uncapped leading barbed ends per unit arc length of the cell boundary, but the number of filaments of given orientation crossing the segment $[x, x + \Delta x]$ near the front divided by Δx (Fig. 1). We also introduce the total density of actin filaments, $p(x,t) = p^+(x,t) + p^-(x,t)$, and the total number of leading edge filaments with uncapped barbed ends: $\bar{P}(t) = \int_{-L}^{L} (p^+(x,t) + p^-(x,t))\,dx$. The intensity measured by rhodamine staining is proportional to the number of polymerized actin monomers per unit area. In our model, this number of polymerized actin monomers per unit area is $p(x,t)/\cos(35°)$, so the experimentally measured actin density is proportional to the number density, $p(x,t)$.

Model equations for actin density

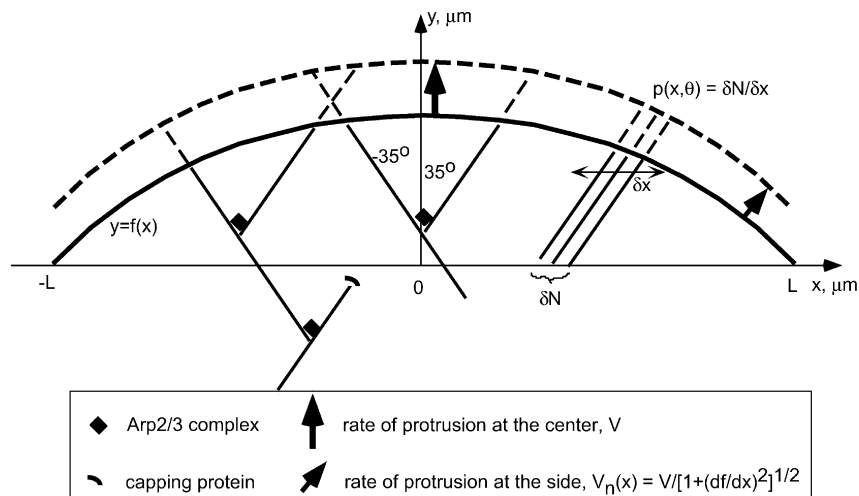The following equation governs the dynamics of the actin density at the leading edge:

$$\underbrace{\frac{\partial p^\pm}{\partial t}}_{\text{density change}} = \underbrace{\mp \frac{\partial}{\partial x}\left(v^\pm p^\pm\right)}_{\text{lateral flow}} + \underbrace{\beta b_{1,2}(p^\mp)}_{\text{branching}} - \underbrace{\gamma p^\pm}_{\text{capping}} \tag{1}$$

The first term on the right-hand side describes the *lateral drift* of the growing barbed ends along the leading edge. This drift is due to the fact that when the lamellipodial boundary extends forward, a tip of a straight filament tilted relative to the boundary glides along the edge, assuming that the tip keeps up with the edge (Small 1994). (This assumption is justified using the following mechanical argument: an uncapped barbed end lagging behind would grow without resistance and would catch up with the boundary, where the filaments are slowed down by the membrane resistance.) The corresponding rate of the flow, $v^\pm$ ($\mu m\,s^{-1}$), is easy to find from the geometric considerations (see Fig. 1):

$$v^\pm(x,t) = \frac{\mp(\partial f/\partial t)}{(\partial f/\partial x) - \cot(\theta_\pm)} \tag{2}$$

In the special case of the steady protrusion of the leading edge with constant shape and velocity V:

Fig. 1 Mathematical model. The leading edge is described by the solid curve $y = f(x)$. We describe the actin network along the cell front between the lateral edges, $-L < x < L$. When the cell movement is steady, the shape of the leading edge is constant (*solid and dashed curves*). According to the graded radial extension model, the local protrusion rate is normal to the boundary and graded spatially, so that it decreases toward the sides. The barbed ends of the straight growing actin filaments (*solid segments*) push the leading edge forward. Before a filament gets capped and disappears from the leading edge, its tip remains localized at the leading edge along which it glides laterally while growing (*dashed segments*). Nascent filaments nucleated with the help of Arp2/3 complexes and branching out from the existing filaments substitute for those lost due to capping. The branching angle between "mother" and "daughter" filaments is approximately 70°. We approximate the angular distribution of the actin network by two populations of left- ($-35°$) and right- ($35°$) pointing filaments. The filament number density, $p(x,\theta)$, is defined as the number of filaments of a given orientation divided by the length of the segment parallel to the x-axis which they intersect

$$v^{\pm}(x) = \frac{V}{1.42 \mp f'(x)} \tag{3}$$

Here $f'(x) = df/dx$ is the slope of the leading edge, and $\cot(35°) \approx 1.42$. Our observations show that the slope of the leading edge of the keratocyte is not steep: $|f''(x)| < 1.42$ for all x, and the lateral velocity is always finite.

The second term on the right-hand side is responsible for the nucleation of nascent growing barbed ends as a result of branching with the rate constant β (s^{-1} µm^{-1}). (The indices 1,2 and functions $b_{1,2}$ correspond to two different models of branching, discussed below.) Note that in the branching process, nascent right- (left-) pointing filaments appear on the left- (right-) pointing existent filaments; thus the rate of change of density, $p^{\pm}$, is proportional to $p^{\mp}$. The last term on the right-hand side describes the loss of the growing barbed ends due to capping with the rate constant γ (s^{-1}).

The boundary conditions to accompany Eq. (1) are based on the model assumption that no right- (left-) pointing filaments emerge from the left (right) lateral edge:

$$p^{-}(L) = 0, \quad p^{+}(-L) = 0 \tag{4}$$

"Global" and "local" regulation of actin dynamics

The capping and branching processes are mediated by capping proteins and the Arp2/3 complexes, respectively. These proteins associate with F-actin at the front and are subsequently released elsewhere in the lamellipodium in the process of filament disassembly. After that they are recycled to the front, either by diffusion or by molecular motors or both, and interact transiently with other signalling molecules at the leading edge. In the absence of detailed information about these processes, we have to use theoretical arguments to specify the capping and branching rates.

Simulations of the model equations (1, 2, 3, 4) show that these rates cannot be uncoupled from the actin density. If $b_{1,2}(p^{\mp}) = p^{\mp}$ (then the dimension of β is s^{-1}) and $\beta < \gamma$, then the filaments are capped faster than they branch, and they go extinct. On the other hand, if $\beta > \gamma$, the filaments proliferate without limit, and even the lateral flow does not bind the actin density from above. The most natural assumption is that the cell regulates the effective rates to achieve a stable equilibrium: either the capping rate increases at high F-actin density, or the branching rate decreases, or both.

Let us consider two simple scenarios. We will assume that the capping rate is constant, while the branching rate is limited by an effective rate of activation of the Arp2/3 complex at the leading edge. In the first, *local* scenario, a constant number β of nascent filaments are nucleated per second per micron of the cell boundary. Assuming that there is an equal probability for an activated Arp2/3 complex to bind to a filament of any orientation, the following formula defines the function b_1 introduced in Eq. (1):

$$b_1(p^{\mp}) = \frac{p^{\mp}}{p^{+}(x,t) + p^{-}(x,t)} \tag{5}$$

In the second, *global* scenario, a constant number βL of nascent filaments are nucleated per second over the whole leading edge. Also, each filament has an equal probability of branching *per unit length, independently of the filament's location*. In this case, the following formula defines function b_2 introduced in Eq. (1):

$$b_2(p^{\mp}) = \frac{Lp^{\mp}}{\bar{P}}, \quad \bar{P} = \int_{-L}^{L}(p^{+}(x) + p^{-}(x))dx \tag{6}$$

where $\bar{P}$ is the total number of growing filaments at the cell's front.

Note that in both cases the average length of a capped filament is:

$$l = V/(\gamma \cos(35°)) \tag{7}$$

because when the cell glides steadily with velocity V, each filament elongates at the rate $V/\cos(35°)$, and the elongation terminates on average in $1/\gamma$ seconds. The global scenario predicts that in the steady state each filament has on average one branching point. On the other hand, according to the local scenario, branching points are distributed uniformly over the leading edge, so there will be more branching points per filament at locations with lower F-actin density.

The local model would be true if, for example, β Arp2/3 complexes are activated per second at one micron of the leading edge and are immediately associated with the growing filaments (and the length of the filaments is not rate limiting). On the other hand, the global model would be valid if, upon activation, the Arp2/3 complexes are spread evenly along the leading edge (by diffusion or otherwise) before associating with F-actin (again, the length of the filaments is not rate limiting). Let us mention that in this work we do not hypothesize any explicit scenario, but rather assume a highly plausible yet unidentified regulation mechanism maintaining dynamic equilibrium for the actin population. We investigate two of the simplest mathematical formulations implying some such mechanism.

Model equations for leading edge dynamics

Under physiological conditions, the elastic polymerization ratchet model gives the following formula for the rate of protrusion of the leading edge: $V_n \approx V_0 \exp(-f_r\delta/k_BT)$, where V_0 is the free polymerization velocity, f_r is the membrane resistance force per filament, δ is the length increment of the fiber at one instance of monomer assembly, and k_BT is the thermal energy (Mogilner and Oster 1996). Here we assume that the protrusion is locally normal to the edge (Lee et al. 1993b), and neglect the dependence of δ on the slope of the leading edge, which is justified when the slope is not steep. We will also assume that effective membrane resistance to protrusion, F (pN µm^{-1}), is constant along the leading edge and is independent of density and velocity. This is likely since some part of the F-actin density, p_0, participating neither in the force generation nor in resistance, exists at the cell front. Capped filaments with their capped ends close to the front could contribute to this density. We will assume that $p_0 =$ const. This density has to be subtracted from the total density. The parameter p_0 will be found from comparison with the experimental data. We will also assume that the load is equally divided amongst the force-generating filaments, each bearing a share $f_r = F/(p(x)-p_0)$, where we neglect the insignificant dependence on the slope of the leading edge. Introducing the notation $\omega = F\delta/(k_BT)$ for the scaled resistance per unit length of the leading edge, we can re-write the theoretical density–velocity relation in the form:

$$V_n(x) \approx V_0 \exp\left(-\frac{\omega}{p(x) - p_0}\right) \tag{8}$$

The density–velocity relation depends on three non-dimensional model parameters, (V_0/V), $w = \omega/p(0)$ and $\psi_0 = p_0/p(0)$. In terms of these parameters, the theoretical density–velocity relation can be written in the form: $(V_n(\psi)/V) = (V_0/V)\exp(-w/(\psi-\psi_0))$, where $\psi = p(x)/p(0)$. This formula defines the graded rate of change of the leading edge shape as a function of the local actin density.

Characteristic scales

The natural spatial scale in the system is the distance from the center to the lateral edge of the lamellipodium, L. We choose the average time of the nascent filament growth before capping, $1/\gamma$, as the time scale for computations. The actin density scale is defined by the balance between the branching and capping, β/γ. In the Appendix we scale and non-dimensionalize the model equations. The important conclusion of the scaling procedure is that the actin density profile is determined by the single non-dimensional parameter $\varepsilon = V/(\gamma L)$. This parameter can be interpreted either as

the ratio of the average filament's length (Eq. 7) to the cell size, or as the ratio of the rate of the barbed end disappearance due to the lateral flow, V/L, to the capping rate, γ. Only the amplitude, but not the shape, of the actin density depends on the branching rate. At the observed cell speed and size ($L \approx 20$ μm, $V \approx 0.25$ μm s^{-1}), $V/L \approx 0.0125$ s^{-1}. Then, comparing the model's solutions to the experimental data, we can estimate ε and the capping rate $\gamma = V/\varepsilon L$.

Results

The description of the results is organized as follows. In the first two subsections ("Shape and motion of the cell are steady: experiment" and "Actin filament density at the leading edge: experiment") we report experimental observations of cell shape and actin density at the leading edge. In the following subsection ("Flat leading edge: theory") we describe analytical and numerical stationary solutions of the actin density equations in the simple hypothetical case of the flat leading edge. These solutions allow us to build an understanding of the actin density behavior and to choose the local branching model over the global one. We analyze theoretically the effect of the steady leading edge shape on the actin density in the next subsection ("How shape of the leading edge determines the actin density: theory"), which gives us clues about the stability of protrusion. We use the experimentally observed cell shape and computer simulations to derive steady actin density distributions and compare them to the corresponding experimental results in the following

subsection ("Comparison of theory and experiment"). This comparison allows us to estimate the effective capping rate. In the next subsection ("How actin density shapes the leading edge: theory and experiment") we estimate unknown model parameters by fitting the density–velocity relation (Eq. 8) to local protrusion rates found from the observed cell shapes and the graded radial extension theory. Finally, we use the estimates of the model parameters in the last subsection ("Evolution and stability of the coupled (actin density/cell shape) system: theory") to solve numerically the coupled dynamic model equations for the actin density and cell shape.

Shape and motion of the cell are steady: experiment

Two of the most important features of keratocytes for the purposes of this study are the permanence of their "fan-like" shape and the persistent character of their "gliding" motion (Lee et al. 1993a). Since these features are crucial for our model, we explored them quantitatively. From cell contours, variations of the shape of the leading edge were hardly detectable by inspection (Fig. 2a). Fluctuations in the shape can be measured by recording the difference in area, ΔF_i, between the leading edge of the cell at time t_i and the leading edge of the time averaged cell shape (Fig. 2b). During the movement, the cells exhibited slight lateral displacements, so the positions of their lateral boundaries changed irregularly with time. To record the changes of area at the leading edge only and to exclude the changes due to the lateral displacement of the cell and the retraction at the rear, the measurement was restricted to a strip (dashed vertical lines in Fig. 2) parallel to the direction of motion and between the rightmost position of the left boundary of the cell and the leftmost position of the right boundary of the cell. The (temporal) average of the area differences for the cell shown turned out to be just 1.85% of the total area of the cell of average shape. Freely locomoting cells with smooth lamellipodia lacking folds and ruffles usually exhibited difference areas below 3% of the total

Fig. 2 Persistence of the shape and velocity of keratocyte. (**a**) Contours of a fish keratocyte taken from phase images at time intervals of 4 s. Variations of the shape are particularly small at the leading edge. (**b**, **c**) Using the images in (**a**) we derived the time-averaged cell contour (*solid curve*) and measured difference areas ΔF (*shaded*) between the average contour and successive frames shown in (**a**) (the *dashed curve* is one example). The *dashed straight lines* indicate the positions of the lateral edges of the lamellipodium. To disregard the shape changes due to lateral displacement of the cell, ΔF is evaluated for the portion of the leading edge between these lines. This area fluctuates about 1.85% (and never exceeds 3.5%) of the total cell area
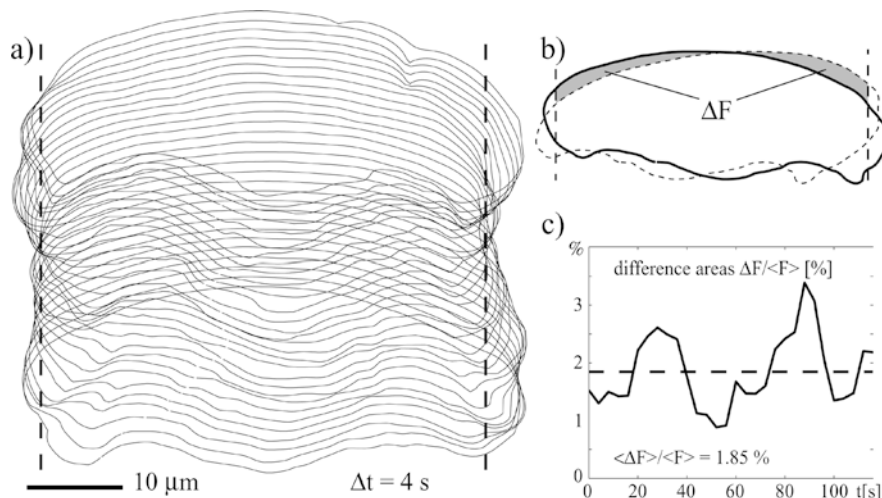
average area. To compare: for a flat leading edge constructed in such a way as to minimize ΔF, the corresponding value would be 8.5%. Thus, the temporal variation of the shape of the leading edge is smaller than the difference between the average shape and the flat leading edge, indicating that the specific curved shape of the edge is conserved with a high degree of precision. Variations of ΔF with time are shown in Fig. 2c. No systematic deviations from the average were detected.

Actin filament density at the leading edge: experiment

Since protrusion is believed to be driven by actin polymerization, the actin density pattern at the leading edge is likely to provide an insight into the mechanism of shape stability. Fluorescence microscopy revealed that actin filament density at the leading edge of a keratocyte exhibited a maximum in the central part of the cell and decreased towards the lateral edges (Fig. 3a, c). Actin density profiles showed significant local fluctuations and variability from cell to cell, comparable to the variability

in cell shape and size (Fig. 3b, c). Nevertheless, the overall shape of the actin density profile with the maximum in the middle was characteristic for most regularly shaped keratocytes.

In order to test if the observed actin density profiles are related to the dynamics of actin polymerization, the cells were treated with a low concentration (0.2 μM) of cytochalasin D, a drug that, similar to actin-capping proteins, blocks actin polymerization at the barbed filament end. At the given concentration of the drug, actin polymerization was not inhibited completely and the rate of advance of the lamellipodia was only reduced by about 30% as compared to the control. However, the actin density profiles became flat, without the maximum at the middle, and the shape of the leading edge became irregular (Fig. 4). This experiment suggested a close relationship between actin polymerization dynamics, filament density distribution and the shape of the leading edge.
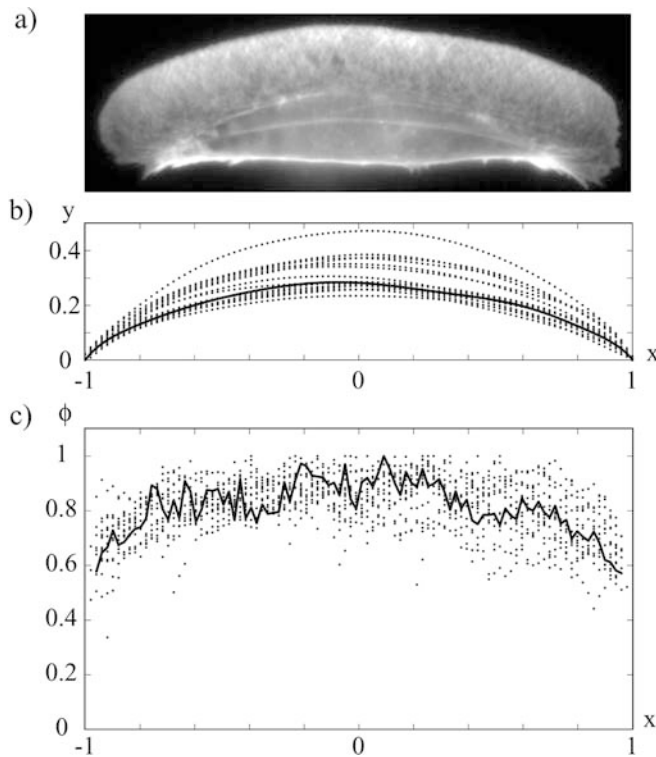

Fig. 3 Actin distribution in keratocyte lamellipodia. (a) Fish keratocyte stained for F-actin with rhodamine phalloidin. (b) Contours of the leading edges are plotted for 15 cells (*dashed curves*) between the lateral edges ($x = \pm 1$; the length scale is half the width of the cell, L; the y-coordinate is also scaled by L). The *solid curve* is the leading edge profile of the cell shown in (a). (c) Along the leading edge, the intensity (proportional to the actin density, φ; normalized so that the maximal observed density is 1) is plotted for 15 cells (*dots*). Despite significant fluctuations, it is seen that the density is highest in the middle of the cell and decreases toward the lateral edges. The *solid line* is the measured intensity for the cell shown in (a)
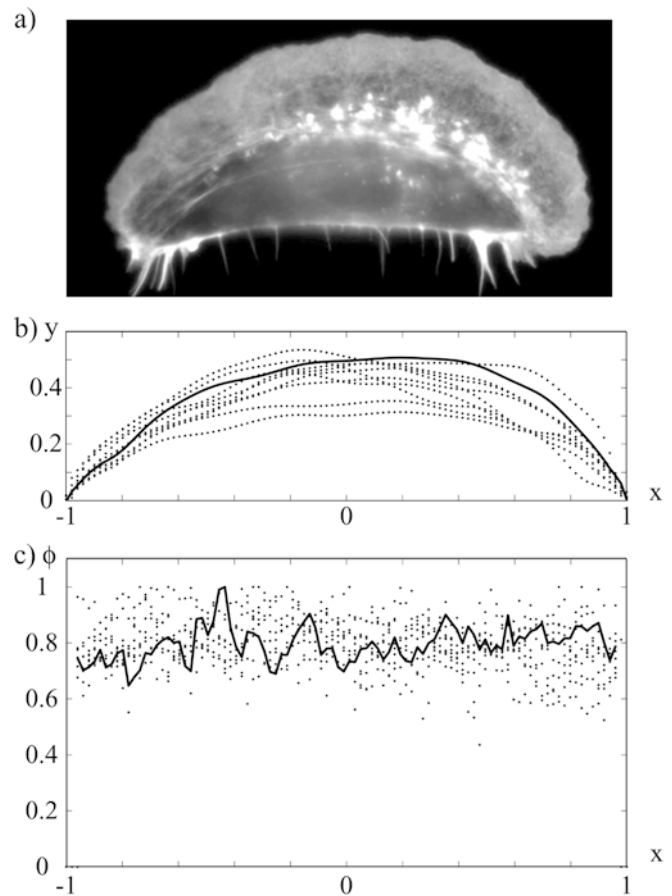

Fig. 4 Actin distribution in the cytochalasin treated cells. (a) Fish keratocyte treated with cytochalasin and stained for F-actin with rhodamine phalloidin. The leading edge contours (b, *dashed*) and the actin density (c, *dots*) for eight cells treated with a low concentration (0.2 μM) of cytochalasin D. (x, y, φ are as in Fig. 3.) *Solid lines* show the data for one of the cells. Both cell boundary and actin density are less regular than those in Fig. 3. The average density profile is flat

Flat leading edge: theory

Let us consider a case of the flat leading edge moving forward with constant velocity. This example can be analyzed easily and helps us to develop an understanding of the actin dynamics. In the limiting cases of very fast and very slow capping, we find approximate stationary solutions of the model equations (1, 2, 3, 4, 5, 6) (see Appendix):

1. Slow capping: $\gamma \ll 0.01$ s^{-1}, $\varepsilon \gg 1$; actin density has the following form (Fig. 5a):

$$\underbrace{p \approx \frac{\beta L}{\sqrt{2}V}\sqrt{1 - \left(\frac{x}{2L}\right)^2}}_{\text{local model}}, \quad \underbrace{p \approx \frac{\beta L}{\sqrt{2}V}\cos\left(\frac{\pi x}{4L}\right)}_{\text{global model}} \quad (9)$$

2. Fast capping: $\gamma \gg 0.01$ s^{-1}, $\varepsilon \ll 1$; actin density has the following form (Fig. 5c):

$$\underbrace{p \approx \frac{\beta}{\gamma}}_{\text{local model}}, \quad \underbrace{p \approx \frac{\pi\beta}{4\gamma}\cos\left(\frac{\pi x}{2L}\right)}_{\text{global model}}, \quad (10)$$

at $-L + \varepsilon < x < L - \varepsilon$

3. In the intermediate case of $\gamma \approx 0.01$ s^{-1}, $\varepsilon \approx 1$, we solved the model equations numerically. The corresponding actin density is shown in Fig. 5b.

At all values of the model parameters (Table 1), the following features characterize actin density, $p(x)$: (1) actin density is symmetric, $p(x) = p(-x)$; (2) actin density has a maximum at the center of the leading edge; the density decreases to the sides, because according to the boundary conditions there are very few right- (left-) pointing filaments at the left (right) side; (3) the actin density profile is convex. All these properties compare favorably with the experimental data (Fig. 2c). The most notable difference in the density profiles evolving at different capping rates is the ratio of the density at the

Fig. 5 Actin density profiles for the flat leading edge moving forward with constant velocity (x, φ are as in Fig. 3). Asymptotically stable stationary solutions of the model equations for the density of the right-pointing (*dashed*) and left-pointing (*dash-dotted*) filaments and total density (*solid*) are plotted. The densities are normalized so that the total density at the center is unity. The left and right columns illustrate the solutions of the global and local models, respectively. Total actin density is symmetric, convex down, has a maximum at the center, and decreases to the sides. The ratio of the total actin density at the center to that at the sides increases with the growth of the capping rate. The actin profiles are qualitatively similar in the global and local models at slow and intermediate capping rates (**a, b**). When the capping rates are fast, the total actin density in the global model has a steep slope along the leading edge, while in the local model the density has a flat profile with sharp drops at the sides
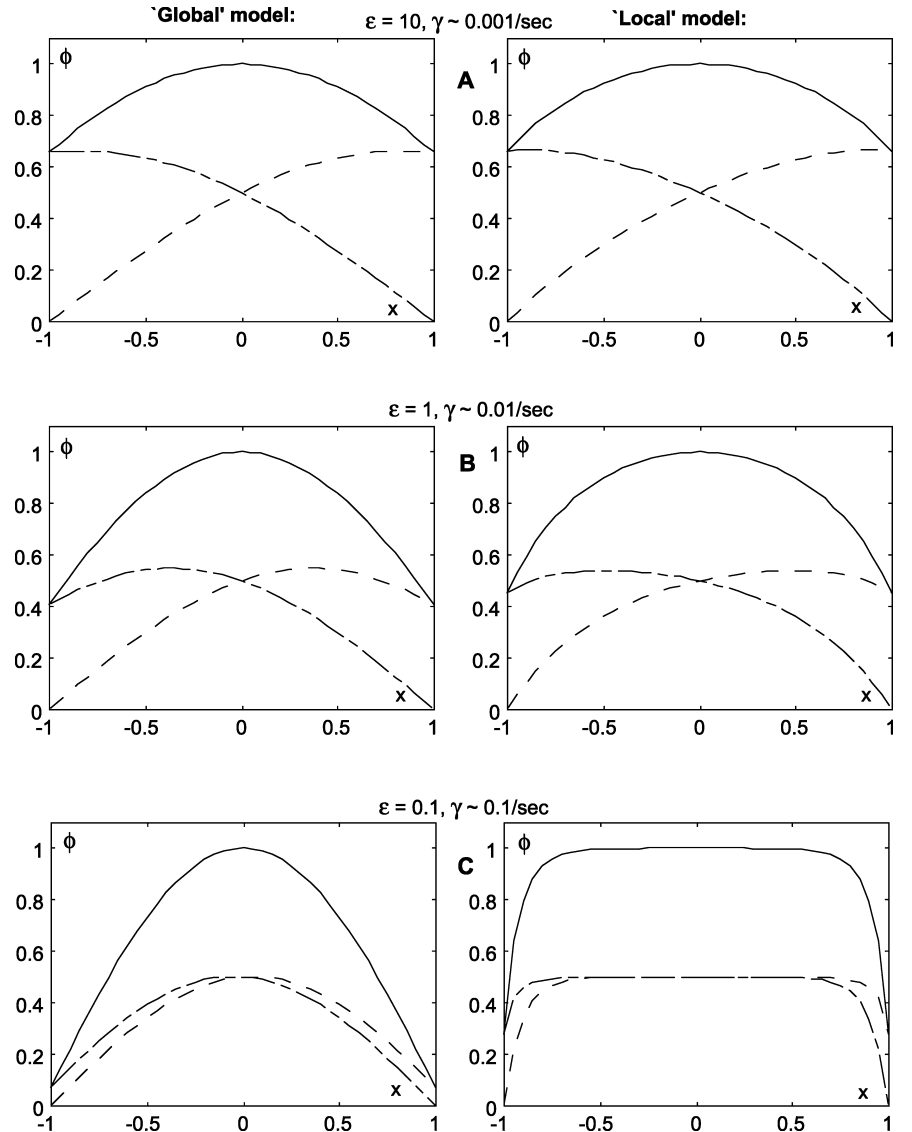
Table 1 Model variables and parameters

Symbol	Range of values	Meaning
t	Tens of seconds	Time
x	Tens of μm	Coordinate parallel to the leading edge
y	Few μm	Coordinate parallel to the direction of protrusion
$y = f(x,t)$	Few μm	Function describing the profile of the leading edge
$\theta_\pm$	$\pm 35°$	Orientation of actin filaments relative to the direction of protrusion
L	Tens of μm	Coordinate of the inner boundaries of the lateral edges of the lamellipod
$p^\pm(x,t)$	Hundreds per μm	Densities of right- and left-pointing actin filaments with uncapped barbed ends at the leading edge
$P(t)$	Thousands	Total number of the leading edge actin filaments
$v^\pm$	Tenths of μm per second	Rate of the lateral flow of the leading edge actin filaments
V	Tenths of μm per second	Rate of cell protrusion
V_0	Tenths of μm per second	Free polymerization rate
V_n	Tenths of μm per second	Local rate of cell protrusion
$b(p^\pm)$	–	Functional dependence of branching on the actin density
β	Tens per μm per second	Branching rate
γ	Tenths per second	Capping rate
l	μm	Average filament length
F	Tens of pN per μm	Effective membrane resistance
f_r	Tenths of pN	Effective membrane resistance per filament
δ	Few nm	Filament length increment at one monomer assembly
k_BT	4.1 pN nm	Thermal energy
p_0	Tens per μm	Threshold actin density below which no protrusion occurs
ω, w	–	Scaled membrane resistance
ψ, ψ_0	–	Scaled actin density

center to that at the lateral edges, $p(0)/p(\pm 1)$. This ratio is the lowest, $p(0)/p(1) = \sqrt{2}$, in the limit of slow capping (Fig. 5a), because the long actin filaments extend across the whole lamellipodium in this case and attenuate local density variations. This ratio increases at intermediate values of the capping rate, and in the limit of fast capping it becomes very large, of the order of $1/\varepsilon$ (Fig. 5c). The reason is that when capping is fast, the filaments are short, actin growth has a local character, and the amount of nucleated F-actin is small near the lateral edges because of the boundary conditions and branching dynamics.

The actin profiles are qualitatively similar in the global and local models at slow and intermediate capping rates (Fig. 5a, b), because the long actin filaments in these cases "globalize" the actin dynamics. However, at fast capping rates the profiles are very different (Fig. 5c). In the local model, the actin density along the edge is determined by the balance between constant nucleation and capping rates, and is thus constant (other than closer than ε to the edges, where the density is not built up). However, in the global model, the nucleation is not distributed uniformly along the leading edge. A greater number of filaments at the center consumes a greater part of the nucleation factors, and the density decreases steadily and significantly from the center toward the sides. Our observation of the effect of cytochalasin D on actin density can be interpreted as an indication that a greater rate of capping maintains a flatter density profile (providing that the drug's inhibitory effect is equivalent to capping). This interpretation supports the local model over the global one. In what follows, we use the local model to generate theoretical results that we compare with the experimental results. Note that the fast capping limit is biologically relevant, according to previous estimates of the capping rates (see Pollard et al. 2000and references therein). Intermediate and slow capping rates (in the mathematical sense) correspond to filaments stretching across the whole cell and not being capped, but rather terminated at the lateral sides. Such rates are unlikely.

How shape of the leading edge determines the actin density: theory

We used computer simulations to analyze the effect of the steady shape of the leading edge on the actin density. At fast capping rates, the smooth convex shape of the leading edge changes the actin density only slightly, making it more convex (Fig. 6a). Figure 6b gives an example of the influence of a perturbation of the shape at different capping rates on the density profile. At high capping rates the actin density increases at places of leading edge outgrowth, and decreases at indentations. The lower capping rates result in generally smoother actin density profiles.

As mentioned earlier, we hypothesize that there is a positive correlation between actin density and the local protrusion rate: greater actin density leads to faster protrusion. This has important consequences for the stability of the lamellipodial shape. If actin filaments are depleted locally as a result of a flattened or indented leading edge, then the protrusion rate is reduced at this place causing the indentation to increase, which further

572

Fig. 6 Influence of the shape of the leading edge on the actin density (*x, y, φ* are as in Fig. 3). Asymptotically stable stationary solutions of the model equations for the total filament density in the local model are plotted. (**a**) The actin density profile (*dashed*) near the flat leading edge (not shown) is less convex than the profile (*solid*) near the curved, convex leading edge (*stars*). (**b**) The leading edge is perturbed by the outgrowth at the left (*stars*). At a higher capping rate (*dashed curve*) an indentation of the leading edge leads to a local depletion of filaments, while a front's outgrowth causes an accumulation of actin. The correlation between the density and extension rate can lead to the instability of the cell front in this case. At a low capping rate (*solid curve*) the actin density is less perturbed, suggesting that the shape of the lamellipodium is more stable at low capping rates
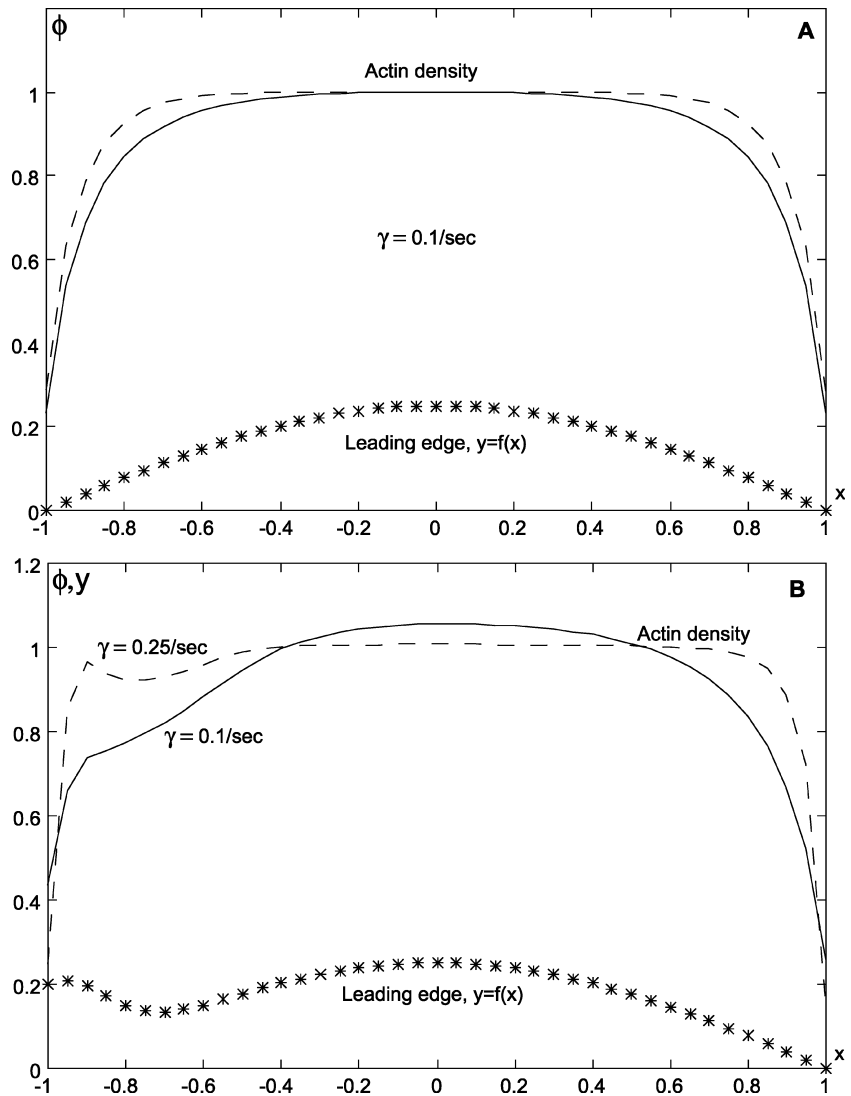
decreases the density. A similar argument in the case of an outgrowth at the leading edge suggests the existence of a positive feedback, which could destabilize the front. (Of course, more adequate modeling has to take into account the effect of membrane tension, which stabilizes the cell front.) As Fig. 6b demonstrates, this is the case for high capping rates. On the other hand, at low capping rates the density distribution is smoother, which helps to maintain a regular shape of the leading edge. A possible connection could be made to the irregular shape of cells that were treated with cytochalasin D, which effectively increases the capping rate: we observed that the lamellipodial shape is much less stable and undergoes large fluctuations (Fig. 4).

Comparison of theory and experiment

For a set of 15 fish keratocyte cells, we evaluated the shapes of the leading edges of the lamellipodia ($y = f(x)$)
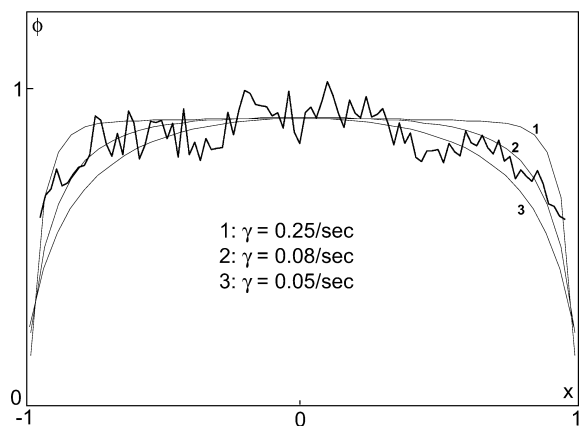

Fig. 7 Comparison of theory and experiment. The local model equations for the actin density were solved at different values of the capping rate for the steady shape of the leading edge shown in Fig. 3b. The asymptotically stable stationary density profiles (curves *1, 2,* and *3* normalized as explained in the text) are fitted over the measured density (Fig. 3c) (*x, φ* are as in Fig. 3)

and the actin filament density (Fig. 3b, c). We fitted the theoretical density curves for different capping rates over the characteristic experimental profiles (Fig. 7). Theoretical results were normalized so that the theoretical density amplitude at the center is the same as the experimental density averaged over central region of the lamellipodium (in the interval $-0.25 < x < 0.25$). Rates of capping of the order of $\gamma \approx 0.1$ s^{-1} gave the best fit. Faster (slower) capping rates result in too flat (convex) density profiles. Note that our data allow only a very rough order of magnitude estimate of the capping rate. The visual impression from Fig. 7 is that $\gamma = 0.08$ s^{-1} gives a better fit than $\gamma = 0.05$ or 0.25 s^{-1}. More rigorous statistical analysis was not conclusive.

How actin density shapes the leading edge: theory and experiment

According to the graded radial extension model (Lee et al. 1993b), the boundary of the steadily gliding keratocyte extends locally in the direction normal to the boundary. In order to maintain constant cell shape, the extension rate has to be constant in time and graded in space according to the following formula:

$$v_n(x) = V/\sqrt{1 + (f'(x))^2} \tag{11}$$

Here $V_n(x)$ is the rate of normal protrusion at the point of the leading edge with coordinates $(x, y = f(x))$. We measured the shape of the leading edge $y = f(x)$ and took its numerical derivative to use Eq. (11) and obtain an approximation for the normal velocity (Fig. 8b). In order to investigate the relation between actin density and protrusion velocity, we plotted these values of the normal velocity and experimental values of the actin density

(profiles shown in Fig. 8a, b) at the grid points in the non-dimensional interval $-1 < x < 1$.

The corresponding density–velocity data points are plotted in Fig. 8c. Given that the leading edge is relatively flat in its middle part, most points are gathered in a region near maximal velocity and maximal density. These data suggest that velocity is an increasing function of density saturating to an upper limit at high values of density, which is in agreement with our model (Eq. 8). (When p increases, the power ω/p of the exponential factor converges to zero, and $V \to V_0$.) We estimate the model parameters (V_0/V), ψ_0 and w from Eq. (8) by comparing the experimental density–velocity data with theoretical predictions. Figure 8c shows the theoretical density–velocity curve obtained using Eq. (8) fitted over the data from one cell. Figure 8d shows a plot of two of the three fitting parameters for the cells investigated. The fitting procedure did not converge for 3 out of the 16 cells considered. Removing one outlier, we obtained the following averages for the fitting parameters: $V_0/V = 1.07 \pm 0.04$, $w = 0.033 \pm 0.017$ and $\psi_0 = 0.47 \pm 0.1$. The small variations of parameters ψ_0 and of V_0 support the model assumptions.

The low estimated value of the parameter $w/p(0)$ (equivalently, closeness of V_0/V to unity) implies that the membrane resistance to protrusion in fish keratocytes is relatively low. A rough estimate for the resistance can be obtained if we use the observation (Abraham et al. 1999) that there are a few hundred filaments per micron of the leading edge. Then, the membrane resistance is $F \approx (\omega k_B T/\delta) \times (200\ \mu\text{m}^{-1}) \approx 10$ pN μm^{-1} ($k_B T \approx 4$ pN nm, $\delta \approx 2$ nm). This value agrees with the value of the membrane resistance determined by the splay of the outer membrane leaflet and compression of the inner leaflet (Evans and Skalak 1980). Higher values of the membrane resistance

Fig. 8 Density–velocity relation. (**a**) Measured actin density normalized so that the maximal density is 1 (Fig. 3c; x, φ are as in Fig. 3). (**b**) Local normal protrusion velocity (V_n scaled by V) was computed from the leading edge profile, $y = f(x)$ (Fig. 3b) using Eq. (10) of the graded radial extension model. (**c**) Measured actin density (**a**) and the normal velocity (**b**) are compared at the grid points and plotted as *dots*. The theoretical result (*solid curve*) is fitted over the experimental data (*dots*). (**d**) Parameter values (for two of the three parameters; for 13 cells). V_0 is the free polymerization rate, $w = \omega/p(0)$ is the scaled membrane resistance, and $\psi_0 = p_0/p(0)$ is the scaled fraction of the "background" F-actin
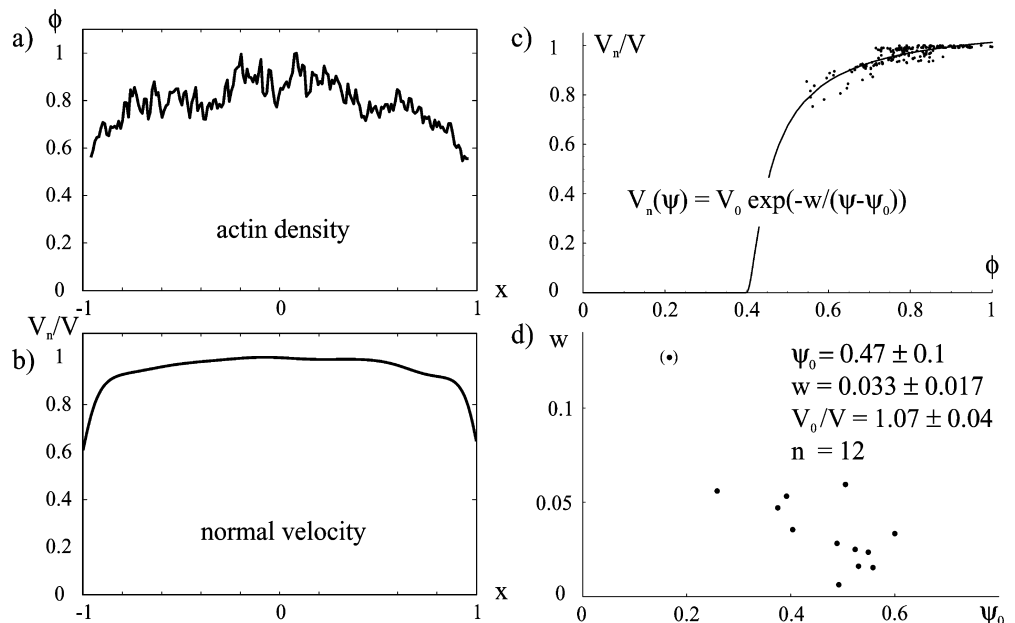
measured in different cells (Dai and Sheetz 1999) can be explained by binding energy dissipation when the links between the actin cortex and membrane are broken as the membrane is pushed forward. These links are probably weak in motile keratocytes.

Evolution and stability of the coupled (actin density/cell shape) system: theory

Equations for actin dynamics depending on the shape of the leading edge (Eqs. 1, 2, 4, 5), together with Eq. (8) for the normal extension rate of the cell boundary as a function of the actin density, form a closed system for the computation of the evolving actin density and shape of the leading edge. To simulate the density and shape, we used the iterative numerical procedure described in the section "Mathematical modeling and comparison to experimental data" and the parameter values $\varepsilon = 0.2$, $V_0/V = 1.07$, $\omega/p(0) = 0.033$ and $p_0/p(0) = 0.37$ (found to provide good fits to the experimental data). The simulations demonstrated that asymptotically stable profiles of the density and leading

Fig. 9 Self-organization of the lamellipodial shape and actin density: Equations for actin filament density coupled with equations describing graded protrusion velocity and leading edge extension were solved simultaneously. We plotted fully evolved asymptotically stable profiles of the leading edge (*top*), actin density (*middle*) and protrusion velocity (*bottom*). In the simulations, we used parameter values $\varepsilon = 0.2$, $V_0/V = 1.07$, $\omega/p(0) = 0.033$ and $p_0/p(0) = 0.37$

edge evolve (Fig. 9). These profiles are comparable to those observed (Fig. 3), so the suggested scenario of the maintenance of the lamellipodial shape is plausible. Numerical experiments with stochastic fluctuations of the branching and capping rates showed that lower capping rates (longer filaments) support a more regular and stable cell boundary.

Discussion

Cell motility is ultimately a mechanical phenomenon, and, as such, has been a subject of biophysical studies and mathematical modeling for a long time. These studies have concentrated either on features of macromolecular assemblies and individual reactions involved in motility (e.g., actin network assembly, rheology of polymer gels) (Janmey et al. 1994; Carlsson 2001; Maly and Borisy 2001; Mogilner and Edelstein-Keshet 2002), or on phenomenological descriptions and modeling of the behavior of the cell as a whole (Huang et al. 1997). However, there have been only a few attempts to connect the molecular and cellular levels of description (Bottino et al. 2002). Perhaps the most natural system in which these levels can be bridged is the leading edge of rapidly moving cells, where actin dynamics are well studied (Borisy and Svitkina 2000; Pollard et al. 2000; Bray 2001).

The fish epidermal keratocyte is perfectly suitable for such modeling because of the stability of its smoothly curved shape, the flatness of the lamellipodium and the steady and persistent character of its locomotion. In keratocytes, the protrusion and contraction events of the motility cycle occur continuously and simultaneously, but there is a clear spatial separation between the two: protrusion is confined to the front of the cell, while contraction occurs at the rear and the extreme lateral edges (Svitkina et al. 1997; Anderson and Cross 2000). Therefore, it is reasonable to hypothesize that the shape of the leading edge of a keratocyte represents the basic shape of the protrusive edge in its purest form, determined solely by the dynamics of the assembling actin network. In other cells the same basic determinants of shape may exist, but the actual shape may be the result of mixed influences of protrusion and retraction processes and thus more difficult to analyze.

The stability of the shape of keratocytes has been phenomenologically described in terms of the graded radial extension model (Lee et al. 1993b), but the mechanism of fine tuning of the extension rate has not been uncovered. The present study is, to our knowledge, the first attempt to analyze the dynamics of the actin filament population in the context of a realistic geometry of the lamellipodium of a motile cell. Making simple geometric and physical assumptions and considering the filament tips' linear elongation and lateral drift along the cell's front, we modeled the dependence of the actin density profile on the rates of capping and on the shape
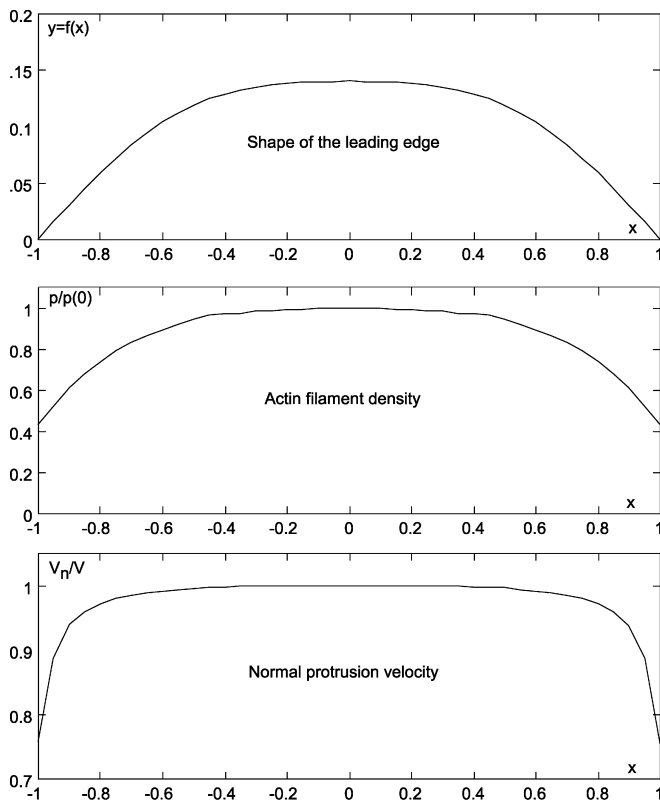
of the leading edge. For a wide range of capping rates and for realistic cell shapes, the model predicted convex actin density profiles with the maximum in the middle of the leading edge. We measured similar actin density distributions experimentally. Fitting the simulated density profiles to the experimental data, we estimated the order of magnitude of the capping rate as ~ 0.1 s^{-1}. At the observed rate of migration ~ 0.25 μm s^{-1}, this predicts that the average length of actin filaments is of the order of a few microns. Although statistical analysis shows that this fitting cannot give a decisive answer about the value of the effective capping rate, best fits were generally achieved at relatively low rates. Our analysis showed that much higher capping rates resulted in flat actin density profiles, which was at odds with experimental observations. Furthermore, treatment with cytochalasin D, expected to increase the effective capping rate, was found experimentally to result in flattening of the actin density profiles. This is consistent with the trend predicted by our model and thus provides further validation to the model.

Our simulations demonstrated that lower capping rates (equivalently, longer filaments) resulted in greater stability of the cell's shape. Qualitatively, this can be explained by the fact that the lateral drift of growing filaments "averages out" local fluctuations of actin density. Thus, lower capping rates could be favorable for persistent steady locomotion: an important preliminary conclusion that has to be tested further by more detailed studies.

Some previous studies suggested that actin capping rates are about one order of magnitude greater than that predicted by our model (~ 1 s^{-1}; see review in Pollard et al. 2000). This could be an indication that the model did not take into account some other factors controlling actin dynamics. However, the estimates of capping from biochemical experiments, as well as electron microscopic images of branching actin networks, have been obtained mostly under transient conditions. Some electron microscopic studies suggested that actin filaments in steadily moving keratocytes could be rather long (Small et al. 1995). In a steadily migrating cell the ends of growing actin filaments remain in the vicinity of the leading edge for a long time, where a number of mechanisms can protect the barbed ends from capping (Hartwig et al. 1995; Schafer et al. 1996; Huang et al. 1999).

Our model predicts that filament length is in the micron range, while an order of magnitude higher capping rates support tenths of a micron long fibers. It has been argued that shorter filaments produce a more branched and robust network. Another argument, from the elastic polymerization ratchet model, is that a single filament longer than 200 nm is too flexible and buckles under membrane resistance (Mogilner and Oster 1996). However, the crosslinking and/or entanglement of long filaments can produce a stiff interconnected network with only the short tips of a fiber bending significantly, and thus withstanding greater resistance. Another important implication of greater filament length is for the turnover of actin. Very fast turnover rates needed for rapidly migrating cells require many F-actin minus ends (Carlier and Pantaloni 1997). Fewer and longer filaments mean less minus ends, so mechanisms of creating minus ends, such as severing (McGrath et al. 2000), could be very important.

Our model would have to be changed drastically if regulatory factors controlling actin assembly (e.g., Arp2/3 complexes, capping proteins, G-actin and actin accessory proteins) were distributed along the leading edge in a non-uniform, graded manner. However, if this is true, the next question arises: how is the distribution of these factors controlled and maintained? In our model, rather than hypothesize about corresponding plausible mechanisms, we made a much simpler geometric assumption of existence of the lateral boundaries at the leading edge, such that there is no influx of F-actin to the cell's center from the sides. The fact that our modeling and experimental results agree qualitatively does not exclude the possibility of more complex spatial regulation, but it shows that even the minimal system lacking such factors can develop a realistic motility pattern.

Further investigation of possible coupling of protrusion and contraction forces, as well as the relation between actin density and protrusion velocity, is necessary to test the validity of our model. In a generic cell, where contraction is not spatially separated from protrusion, both protrusion and contraction velocities may be coupled to actin density, resulting in a more complex relationship between density and shape. Also, careful electron micrography is needed to measure the dependence of angular distribution and branching pattern of the actin network as a function of position along the leading edge. The present study is an initial attempt to combine mathematical modeling with cell biological and biophysical methods in order to dissect the mystery of cell motility.

Appendix: asymptotic analysis of the model equations

Scaling and non-dimensionalization

Introducing the non-dimensionalized variables x/L, γt and $p/(\beta/\gamma)$, we can write the model equations in the case of the steady locomotion in the form:

$$\frac{\partial p^{\pm}}{\partial t} = \mp \in \frac{\partial}{\partial x}\left(v^{\pm}p^{\pm}\right) + \frac{p^{\mp}}{p} - p^{\pm}, \qquad (12)$$

$$p = p^+ + p^-, \text{[local model]}$$

$$\frac{\partial p^{\pm}}{\partial t} = \mp \in \frac{\partial}{\partial x}(v^{\pm}p^{\pm}) + \frac{p^{\mp}}{\bar{P}} - p^{\pm},$$

$$\bar{P} = \int_{-1}^{1} p\, dx \quad \text{[global model]} \tag{13}$$

$$v^{\pm}(x) = \frac{1}{1.42 \mp f'(x)}, \quad \in = \frac{V}{L\gamma},$$

$$p^{+}(-1) = 0, \quad p^{-}(1) = 0 \tag{14}$$

Here, for simplicity, we keep the same notations for non-dimensional variables. In what follows, we investigate the steady-state solutions of these equations, i.e. when the time derivative is equal to zero. We also concentrate on the case of the flat leading edge, $f''(x) = 0$. In this last case, without loss of generality we assume that $v^{\pm} = 1$, which can be justified by re-scaling the protrusion velocity ($f''(x) = 0$).

Slow rate of capping

In this case ($\gamma \ll V/L$, $\varepsilon \gg 1$), the scale of the actin density is defined by the ratio of the branching rate β over the effective rate of fiber disappearance due to the lateral flow, V/L. In the non-dimensional system this means that the scale of actin density is $\sim 1/\varepsilon$. Substituting this new scale into Eqs. (12) and (13) and dropping the negligible capping term (the third term on the right-hand side), we obtain the following steady-state equations:

$$-\frac{dp^{\pm}}{dx} + \frac{p^{\mp}}{\tilde{p}} = 0, \quad \tilde{p} = \begin{cases} \bar{P}, & \text{global model} \\ p, & \text{local model} \end{cases} \tag{15}$$

Let us introduce the function $s = p^{+} - p^{-}$. Adding and subtracting Eqs. (15), we obtain the equations:

$$-\frac{ds}{dx} + 1 = 0, \quad \frac{dp}{dx} + \frac{s}{p} = 0 \tag{16}$$

for the local model. The solutions of these equations can be found easily by first solving the first equation of (16), and then the second one, and by using the conditions that $s(x)$ is an odd function, $p(x)$ is an even function, and $p(1) = s(1)$:

$$s = x, \quad p = \sqrt{2 - x^2} \tag{17}$$

The dimensional form of these solutions is given by Eq. (8). For the global model, adding and subtracting Eqs. (15), we obtain:

$$-\frac{ds}{dx} + \frac{p}{\bar{P}} = 0, \quad \frac{dp}{dx} + \frac{s}{\bar{P}} = 0 \tag{18}$$

Differentiating these equations a second time, we find:

$$\frac{d^2(s, p)}{dx^2} + \frac{(s, p)}{\bar{P}^2} = 0 \tag{19}$$

Using symmetry properties of functions $s(x)$ and $p(x)$, we have:

$$p = A\cos\left(\frac{\pi}{\bar{P}}\right), \quad s = A\sin\left(\frac{x}{\bar{P}}\right) \tag{20}$$

Using the condition $p(1) = s(1)$, we find that $1/\bar{P} = \pi/4$. Finally, integrating $p(x)$ from -1 to 1, we obtain the value of A:

$$\bar{P} = \int_{-1}^{1} p(x)dx = 2A\bar{P}\sin(1/\bar{P}), \quad A = 1/\sqrt{2} \tag{21}$$

The dimensional form of these solutions is given by Eq. (9).

Fast rate of capping

In this case ($\gamma \gg V/L$, $\varepsilon \ll 1$), singular perturbation theory can be used to investigate the local model (Eq. 12). Simple analysis shows that away from two boundary layers of width $O(\varepsilon)$ at the spatial domain's edges, the constant "outer" solution, $p^{\pm}(x) = 0.5$, $p(x) = 1$, gives the leading order approximation. Near the boundaries, re-scaling the spatial variable, $x \to \varepsilon x$, leads to a non-linear system, which cannot be solved analytically. A qualitative analysis shows that the corresponding "inner" solution for $p(x)$ decreases from $p = 1$ inside the spatial interval to $p = O(\varepsilon)$ at the boundaries.

Unlike the local model, the global model (Eq. 13) is not characterized by the boundary layers and has an approximate analytical solution in this limit. Adding and subtracting Eqs. (13), we find:

$$\in \frac{ds}{dx} + \left(1 - \frac{1}{\bar{P}}\right)p = 0, \quad \in \frac{dp}{dx} + \left(1 + \frac{1}{\bar{P}}\right)s = 0 \tag{22}$$

Differentiating these equations a second time, we derive:

$$\frac{d^2(s, p)}{dx^2} = -\frac{\kappa^2}{\varepsilon^2}(s, p), \quad \kappa^2 = -\left(1 - \frac{1}{\bar{P}}\right)\left(1 + \frac{1}{\bar{P}}\right) \tag{23}$$

Solving these equations and using symmetry properties of functions $s(x)$ and $p(x)$ gives:

$$p = A\cos\left(\frac{\kappa x}{\varepsilon}\right), \quad s = B\sin\left(\frac{\kappa x}{\varepsilon}\right) \tag{24}$$

Substituting these solutions into Eq. (22) and using the condition $p(1) = s(1)$, we find that $\bar{P} \approx 1 - (\pi^2\varepsilon^2/8)$, $\kappa \approx (\pi\varepsilon/2)$, $A \approx \pi/4$ and $B \approx \pi^2\varepsilon/16$. Thus, the non-dimensional approximate solution of the local model in this limit is $p = (\pi/4)\cos(\pi x/2)$. The dimensional form of the solutions of the global and local models in the fast capping rates limit are given by Eq. (10).

References

Abercrombie M (1980) The crawling movement of metazoan cells. Proc R Soc Lond (Biol) 207:129–147

Abraham VC, Krishnamurthi V, Taylor DL, Lanni F (1999) The actin-based nanomachine at the leading edge of migrating cells, Biophys J 77:1721–1732

Anderson KI, Cross R (2000) Contact dynamics during keratocyte motility. Curr Biol 10:253–260

Bernheim-Groswasser A, Wiesner S, Golsteyn RM, Carlier MF, Sykes S (2002) The dynamics of actin-based motility depend an surface parameters. Nature 417:308–311

Borisy GG, Svitkina TM (2000) Actin machinery: pushing the envelope. Curr Opin Cell Biol 12:104–112

Bottino D, Mogilner A, Roberts T, Stewart M, Oster G (2002) How nematode sperm crawl. J Cell Sci 115:367–384

Bray D (2001) Cell movements. Garland, New York

Cameron LA, Svitkina TM, Vignjevic D, Theriot JA, Borisy GG (2001) Dendritic organization of actin comet tails. Curr Biol 11:130–135

Carlier MF, Pantaloni D (1997) Control of actin dynamics in cell motility. J Mol Biol 269:459–467

Carlsson AE (2001) Growth of branched actin networks against obstacles. Biophys J 81:1907–1923

Condeelis J (1993) Life at the leading edge: the formation of cell protrusions. Annu Rev Cell Biol 9:411–444

Cortese JD, Schwab B, Frieden C, Elson EL (1989) Actin polymerization induces shape change in actin-containing vesicles. Proc Natl Acad Sci USA 86:5773–5777

Dai JW, Sheetz MP (1999) Membrane tether formation from blebbing cells. Biophys J 77:3363–3370

Edelstein-Keshet L, Ermentrout GB (2000) Models for spatial polymerization dynamics of rod-like polymers. J Math Biol 40:64–96

Evans E, Skalak R (1980) Mechanics and thermodynamics of biomembranes. CRC Press, Boca Raton, Fla., USA

Garcia AI (1994) Numerical methods for physicists. Prentice-Hall, Englewood Cliffs, NJ, USA

Gerbal F, Chaikin P, Rabbin Y, Prost J (2000) Elastic model of Listeria propulsion. Biophys J 79:2259–2275

Hartwig JH, Bokoch GM, Carpenter CL, Janmey PA, Taylor LA, Toker A, Stossel TP (1995) Thrombin receptor ligation and activated rac uncap actin filament barbed ends through phosphoinositide synthesis in permeabilized human platelets. Cell 82:643–643

He H, Dembo M (1997) On the mechanics of the first cleavage division of the sea urchin egg. Exp Cell Res 233:252–273

Huang M, Yang C, Schafer DA, Cooper JA, Higgs HN, Zigmond SH (1999) Cdc42-induced actin filaments are protected from capping protein. Curr Biol 9:979–982

Janmey PA, Hvidt S, Kas J, Lerche D, Maggs A, Sackmann E, Schliwa M, Stossel TP (1994) The mechanical properties of actin gels, elastic modulus and filament motions. J Biol Chem 269:32503–32513

Lee J, Ishiara A, Jacobson K (1993a) The fish epidermal keratocyte as a model system for the study of cell locomotion. In: Jones G, Wigley C, Warn R (eds) Cell behavior: adhesion and motility. Company of Biologists, Cambridge, UK, pp 73–89

Lee J, Ishihara A, Theriot J, Jacobson K (1993b) Principles of locomotion for simple-shaped cells. Nature 362:467–471

Logan JD (1997) Applied mathematics. Wiley, New York

Loisel TP, Boujemaa R, Pantaloni D, Carlier MF (1999) Reconstitution of actin-based motility of listeria and shigella using pure proteins. Nature 401:613–616

Maly IV, Borisy GG (2001) Self-organization of a propulsive actin network as an evolutionary process. Proc Natl Acad Sci USA 98:11324–11329

McGrath JL, Osborn EA, Tardy YS, Dewey CF, Hartwig JH (2000) Regulation of the actin cycle in vivo by actin filament severing. Proc Natl Acad Sci USA 97:6532–6537

Mitchison TJ, Cramer LP (1996) Actin-based cell motility and cell locomotion. Cell 84:371–379

Miyata H, Nishiyama S, Akashi KI, Kinosita K (1999) Protrusive growth from giant liposomes driven by actin polymerization. Proc Natl Acad Sci USA 96:2048–2053

Mogilner A, Edelstein-Keshet L (2002) Regulation of actin dynamics in rapidly moving cells: a quantitative analysis. Biophys J 83:1237–1258

Mogilner A, Oster G (1996) Cell motility driven by actin polymerization. Biophys J 71:3030–3045

Pantaloni D, Clainche CL, Carlier MF (2001) Mechanism of actin-based motility. Science 292:1502–1506

Pollard TD, Blanchoin L, Mullins RD (2000) Molecular mechanisms controlling actin filament dynamics in nonmuscle cells. Annu Rev Biophys Biomol Struct 29:545–576

Rinnerthaler G, Herzog M, Klappacher M, Kunka H, Small JV (1991) Leading edge movement and ultrastructure in mouse macrophages. J Struct Biol 106:1–16

Rottner K, Behrendt B, Small JV, Wehland J (1999) Vasp dynamics during lamellipodia protrusion. Nat Cell Biol 1:321–322

Schafer DA, Jennings PB, Cooper JA (1996) Dynamics of capping protein and actin assembly in vitro: uncapping barbed ends by polyphosphoinositides. J Cell Biol 135:169–179

Small JV (1994) Lamellipodia architecture: actin filament turnover and the lateral flow of actin filaments during motility. Semin Cell Biol 5:157–163

Small JV, Herzog M, Anderson K (1995) Actin filament organization in the fish keratocyte lamellipodium. J Cell Biol 129:1275–1286

Svitkina TM, Borisy GG (1999) Arp2/3 complex and actin depolymerizing factor/cofilin in dendritic organization and treadmilling of actin filament array in lamellipodia. J Cell Biol 145:1009–1026

Svitkina TM, Verhovsky AB, McQuade KM, Borisy GG (1997) Analysis of the actin-myosin 11 system in fish epidermal keratocytes: mechanism of cell body translocation. J Cell Biol 139:397–415

Theriot JA, Mitchison TJ (1991) Actin microfilament dynamics in locomoting cells. Nature 352:126–131

Welch MD, Mallavarapu A, Rosenblatt J, Mitchison TJ (1997) Actin dynamics in vivo. Curr Opin Cell Biol 9:54–61